Quantum Chemical and Master Equation Simulations of the Oxidation and Isomerization of Vinoxy Radicals

Keith T. Kuwata,*,† Alam S. Hasson,‡ Ray V. Dickinson,‡ Erin B. Petersen,† and Lukas C. Valin†

Department of Chemistry, Macalester College, Saint Paul, Minnesota 55105-1899, and Department of Chemistry, California State University, Fresno, California 93740-8034

Received: June 21, 2004; In Final Form: January 17, 2005

The vinoxy radical, a common intermediate in gas-phase alkene ozonolysis, reacts with O_2 to form a chemically activated α-oxoperoxy species. We report CBS-QB3 energetics for O_2 addition to the parent ($^{\bullet}CH_2CHO$, **1a**), 1-methylvinoxy ($^{\bullet}CH_2COCH_3$, **1b**), and 2-methylvinoxy ($CH_3{}^{\bullet}CHCHO$, **1c**) radicals. CBS-QB3 predictions for peroxy radical formation agree with experimental data, while the G2 method systematically overestimates peroxy radical stability. RRKM/master equation simulations based on CBS-QB3 data are used to estimate the competition between prompt isomerization and thermalization for the peroxy radicals derived from **1a**, **1b**, and **1c**. The lowest energy isomerization pathway for radicals **4a** and **4c** (derived from **1a** and **1c**, respectively) is a 1,4-shift of the acyl hydrogen requiring 19−20 kcal/mol. The resulting hydroperoxyacyl radical decomposes quantitatively to form $^{\bullet}OH$. The lowest energy isomerization pathway for radical **4b** (derived from **1b**) is a 1,5-shift of a methyl hydrogen requiring 26 kcal/mol. About 25% of **4a**, but only ∼5% of **4c**, isomerizes promptly at 1 atm pressure. Isomerization of **4b** is negligible at all pressures studied.

I. Introduction

The parent and substituted vinoxy (or oxoalkyl) radicals are key intermediates in both combustion[1−3] and atmospheric[4−7] chemistry. An important source of these species in the troposphere is the reaction of alkenes with ozone (or ozonolysis). Specifically, syn carbonyl oxides produced in ozonolysis isomerize and decompose to yield hydroxyl radicals ($^{\bullet}OH$) and vinoxy radicals:[8−20]

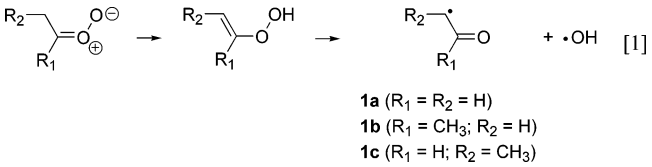

[1]

1a ($R_1 = R_2 = H$)
1b ($R_1 = CH_3$; $R_2 = H$)
1c ($R_1 = H$; $R_2 = CH_3$)

(Note that throughout this paper, **a**, **b**, and **c** will refer to the compounds derived from the parent (**a**), 1-methyl (**b**), and 2-methyl (**c**) vinoxy radicals.) Field studies[21−23] indicate that alkene ozonolysis can be the dominant tropospheric $^{\bullet}OH$ source in urban and rural settings. A complete understanding of the chemistry of the vinoxy radical cogenerated with $^{\bullet}OH$ is therefore important in the development of accurate atmospheric models.

Experiments[24−27] indicate that vinoxy radicals react with moderate facility with molecular oxygen to form α-oxoperoxy radicals:

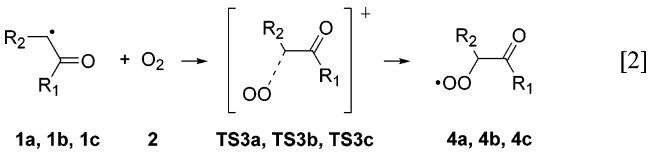

[2]

1a, 1b, 1c **2** **TS3a, TS3b, TS3c** **4a, 4b, 4c**

The kinetics of the reaction of unsubstituted vinoxy radical (**1a**) with O_2, including the pressure dependence of the second-order rate coefficient, has been studied by Gutman and Nelson,[24] by Lorenz et al.,[25] and by Zhu and Johnston.[26] Their data reveal a typical recombination mechanism, with falloff of the second-order rate coefficient being strongest between 10 and 100 Torr. All three groups determined low- and high-pressure-limit rate constants by fitting their data to Troe and co-workers' classic expression.[28]

Miyoshi and co-workers[27] have reported pressure-dependent kinetics measurements for the 1-methylvinoxy (**1b**) and 2-methylvinoxy (**1c**) systems. They have also applied Gaussian-2 (G2)[29] and RRKM[30] calculations to the pressure-dependent data[25−27] to determine energy barriers ($E_{o,rec}$; see Scheme 2 below) and rate constants for the reactions of O_2 with **1a**, **1b**, and **1c**. Miyoshi and co-workers' $E_{o,rec}$ values are significantly lower than the barrier heights predicted[31] by the CBS-QB3[32] and CBS-APNO[33] composite electronic structure methods, with the energies for **TS3b** and **TS3c** below those of the separated methylvinoxy and O_2 reactants. In this paper, we provide detailed quantum chemical evidence that these negative activation energies are artifacts of the G2 method's overestimate of peroxy radical stability.

LIF studies of Gutman and Nelson[24] and Lorenz et al.[25] have provided experimental evidence that the 2-oxoethylperoxy radical (**4a**) decomposes to generate $^{\bullet}OH$. Recent theoretical studies by Lee and Bozzelli[1] and our laboratories[31] attribute $^{\bullet}OH$ formation by **4a** to the intramolecular abstraction of the acyl hydrogen:

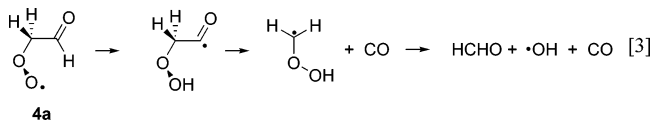

[3]

4a

Our master equation calculations[31] on reaction 3 predicted that for the chemically activated **4a**, $^{\bullet}OH$ formation is quantitative

* Corresponding author. E-mail: kuwata@macalester.edu.
† Macalester College.
‡ California State University, Fresno.

10.1021/jp047299i CCC: $30.25
Published on Web 03/01/2005

at low pressures (less than 10 Torr) and still significant at 1 atm pressure. Alkenes (such as *cis*- and *trans*-butene) whose ozonolysis produces syn acetaldehyde oxide can therefore generate up to two equivalents of •OH via reactions 1 and 3.

In this paper, we quantify the effect of alkyl substitution on the reactivity of the chemically activated α-oxoperoxy radical:

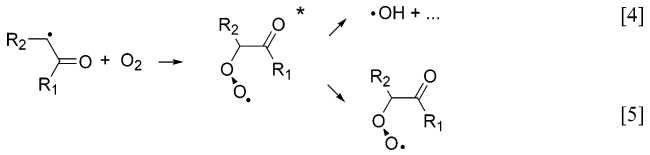

[4] [5]

Based on CBS-QB3 quantum chemical calculations and RRKM/master equation simulations, we determine to what extent prompt isomerization and decomposition to form •OH radical (reaction 4) compete with thermalization (reaction 5) for the 2-oxo-1-propylperoxy (**4b**; $R_1 = CH_3$, $R_2 = H$) and the 1-oxo-2-propylperoxy (**4c**; $R_1 = H$, $R_2 = CH_3$) radicals. This analysis allows us to assess the proficiency of vinoxy radicals as a tropospheric •OH source.

Our calculations also engage Kroll et al.'s[34] report of •OD formation from the ozonolysis of 3-hexenes deuterated at their vinylic positions:

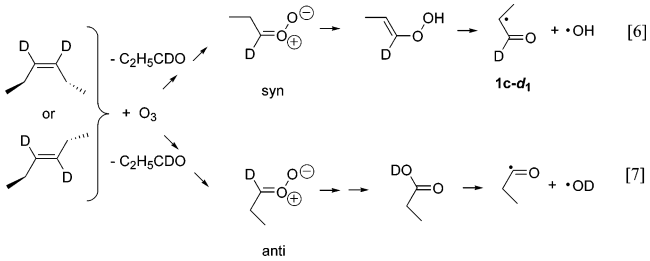

[6] [7]

Kroll et al. argue that •OD radicals are formed in the isomerization and decomposition of anti carbonyl oxides (reaction 7). Based on model calculations on the deuterated parent vinoxy radical **1a-*d*$_1$**, we proposed[31] that the deuterated 2-methylvinoxy radical **1c-*d*$_1$** formed in reaction 6 is another possible source of •OD:

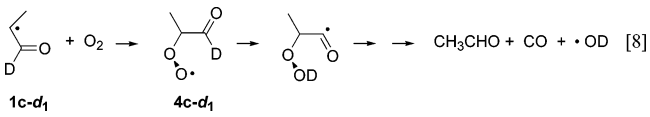

[8]

In this paper, we test this proposal by calculations on the actual intermediate formed in Kroll et al.'s experiments.

II. Theoretical Methods

A. Quantum Chemistry Calculations. All electronic structure calculations were performed with the Gaussian 98 suite of programs.[35] The geometry and energy of each stationary point considered here were determined initially using the B3LYP functional[36,37] and the 6-31G(d,p) basis set.[38,39] The nature of each stationary point was then confirmed by calculating harmonic vibrational frequencies. Each minimum we report has all real frequencies, and each transition structure has one imaginary frequency. Animation of the imaginary frequency, sometimes combined with intrinsic reaction coordinate (IRC) calculations,[40,41] enabled us to associate a given transition structure unequivocally with its reactant and product.

While a popular method for treating atmospheric oxidation reactions,[10−12,16,18−20,31,42,43] the B3LYP method tends to underestimate hydrogen-shift reaction barriers and provide unreliable thermochemical predictions.[31,44−49] Therefore, all of the species considered here were also treated with the CBS-QB3 model chemistry of Petersson and co-workers.[32] This composite method employs optimized geometries and vibrational frequencies obtained at the B3LYP/6-311G(2d,d,p) level, treats electron correlation up to the CCSD(T)/6-31G(d′) level,[50,51] and extrapolates the MP2 energy to the complete basis set limit. Recent studies indicate that CBS-QB3 often, but not invariably, provides excellent agreement with experimental reaction energies and barriers.[44,52−55] The CBS-QB3 relative energies reported here are corrected for differences in zero-point vibrational energy scaled by 0.99.

To study the thermochemistry of peroxy radical formation, we also used Truhlar's MPW1K hybrid density functional,[45,46] Petersson's CBS-APNO method,[33] Pople's Gaussian-2 (G2) and Gaussian-3 (G3) methods,[29,56] and version 2m of Truhlar's Multi-Coefficient G2 (MCG2) method.[57,58] The vibrational contribution to 298 K enthalpies was scaled by 0.9989 for B3LYP/6-31G(d,p),[59] 0.99 for the B3LYP/6-311G(2d,d,p) frequencies used by CBS-QB3,[32] 0.9515 for MPW1K/6-31+G-(d,p),[46] and 0.8929 for the HF/6-31G(d) frequencies used by G2 and G3.[29,56] The MCG2 method does not stipulate any particular method for the calculation of optimized geometries or frequencies. We chose to employ MP2(full)/6-31G(d) geometries (to facilitate comparison with the G2 predictions) and B3LYP/6-311G(2d,d,p) frequencies scaled by 0.99.

B. Statistical Rate Theory Calculations. We used Barker's MultiWell program suite[60,61] to solve the one-dimensional (internal energy) master equation for part of the vinoxy oxidation mechanism. The zero-point-corrected relative energies of all participating species were taken from our CBS-QB3 calculations. Unimolecular rate constants $k(E)$ were computed using Rice−Ramsperger−Kassel−Marcus (RRKM) theory,[30] with the required sums and densities of states being calculated with B3LYP/6-311G(2d,d,p) geometries and unscaled harmonic frequencies. We did not treat low-frequency internal rotations as hindered rotors, and our simulations included only the most stable conformer of each species. These simplifications will affect the numerical accuracy of our results[62,63] but should not detract from the validity of our qualitative conclusions.[64]

Collisional stabilization was treated using the exponential-down model with an average energy transferred per collision ($\langle E_d \rangle$) assumed to be 300 cm^{-1}.[65] The bath gas was taken to be N_2 at 298 K, with Lennard-Jones parameters of $\sigma = 3.74$ Å and $\epsilon = 82$ K.[66,67] Each organic species was assigned ethylene oxide's Lennard-Jones parameters of $\sigma = 4.08$ Å and $\epsilon = 421$ K.[67] Each simulation was run for 1000 collisions to ensure that the pseudo steady state[68] was achieved. However, only ∼100 collisions (corresponding to ∼50 ns at 1 atm pressure) was usually required for the concentrations of all participating species to remain constant to within the numerical noise of the simulation. More details of our rate calculations are given in section III.D below.

III. Results and Discussion

A. Structural Aspects of Vinoxy Oxidation. Figures 1−3 show our B3LYP/6-311G(2d,d,p) predictions for the geometries of all possible conformers of the species in reaction 2. (All

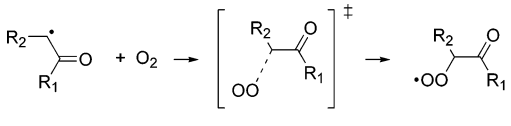

[2]

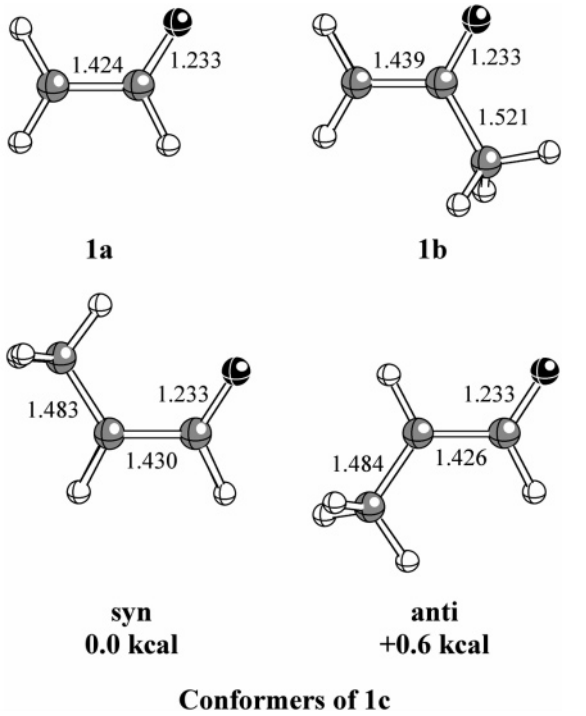

Figure 1. Structures of the parent (**1a**) and methyl-substituted (**1b** and **1c**) vinoxy radicals. Bond lengths (in Å) computed at the B3LYP/6-311G(2d,d,p) level, and relative energies (in kcal/mol) computed with the CBS-QB3 method. Note that in all figures, gray represents carbons, white represents hydrogens, and black represents oxygens.

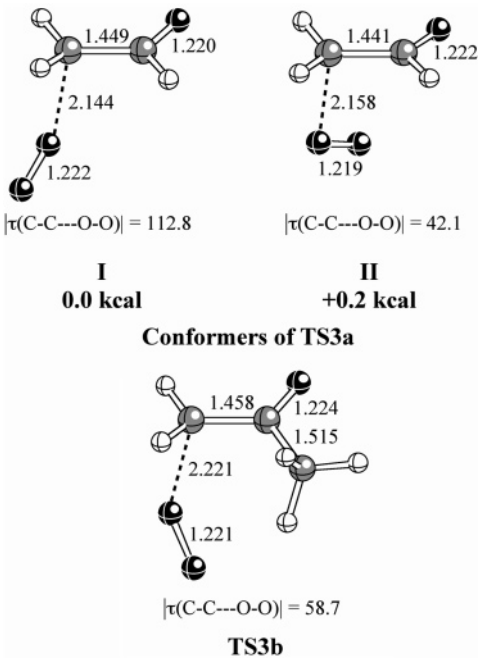

Figure 2. Transition structures for the addition of O_2 to the parent (**TS3a**) and 1-methylvinoxy (**TS3b**) radicals. Bond lengths (in Å) and torsional angles (in degrees) computed at the B3LYP/6-311G(2d,d,p) level, and relative energies (in kcal/mol) computed with the CBS-QB3 method.

structures have been rendered using the Ball & Stick program of Müller and Falk.[69]) When there is more than one conformer for a particular structural isomer, CBS-QB3 relative energies are also shown.

Figure 1 shows the B3LYP/6-311G(2d,d,p) structures of vinoxy (**1a**), 1-methylvinoxy (**1b**), and 2-methylvinoxy (**1c**) radicals. The existence of syn and anti conformers of **1c** has

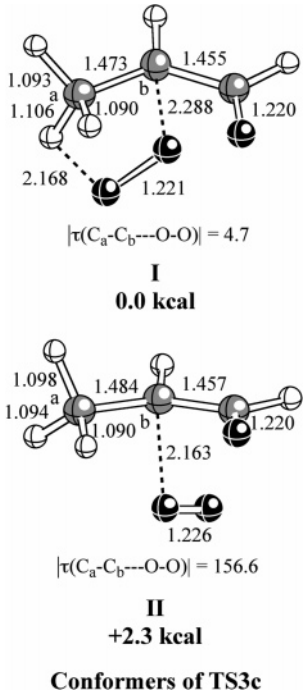

Figure 3. Transition structures for the addition of O_2 to 2-methylvinoxy radical (**TS3c**). Bond lengths (in Å) and torsional angles (in degrees) computed at the B3LYP/6-311G(2d,d,p) level, and relative energies (in kcal/mol) computed with the CBS-QB3 method.

been observed spectroscopically by Weisshaar and co-workers.[70,71] Our calculations predict that although methyl substitution has no effect on the predicted C−O bond length, methyl substitution does increase the distance between the two sp^2-hybridized carbons. In **1b**, this C−C bond is 0.015 Å longer, and in the more stable conformer of **1c**, this bond is 0.006 Å longer. The B3LYP/6-311G(2d,d,p) bond lengths for **1b** and **1c** agree to within 0.01 Å of the CASSCF/6-31G(d,p) predictions of Weisshaar and co-workers.[71] The syn conformer of **1c** is predicted to be 0.6 kcal/mol lower in energy than the anti conformer, in excellent agreement with CASSCF/6-31G(d,p) relative energies.[71] This preference for the syn form is consistent with Wiberg and Martin's[72] prediction that the synperiplanar conformer of propanal is more stable than its anticlinal conformer. Wiberg and Martin attribute this preference to the C═O (permanent) bond dipole's inducing a dipole in the synperiplanar methyl group.

Figures 2 and 3 show the possible conformers of the addition transition structures. The anticlinal (**I**) and synclinal (**II**) conformers of **TS3a** (Figure 2) are nearly identical in energy. Structure **TS3b** (Figure 2) exists as a single conformer. For **TS3c** (Figure 3), the structure with the O_2 synperiplanar to the C_a-C_b bond (**I**) is 2.3 kcal/mol more stable than the structure with the O_2 antiperiplanar to the C_a-C_b bond (**II**). In **I**, the free O atom is rather close to the C−H bond pointing out of the plane of the 2-methylvinoxy radical (r(H- - -O) = 2.168 Å). This proximity permits the donation of electron density from the π^* HOMO of O_2 to the σ^* orbital of the interacting C−H bond. This favorable interaction preferentially lowers **I**'s energy. Evidence for this interaction includes the following: (1) the O−O bond length is 0.005 Å shorter in **I** than in **II**; (2) the interacting C−H bond in **I** is ∼0.01 Å longer than the other two C−H bonds on the 2-methyl substituent; (3) the C−H stretch frequency of the interacting bond in **I** is 140−210 cm^{-1} to the red of the other two C−H stretches in **I**.

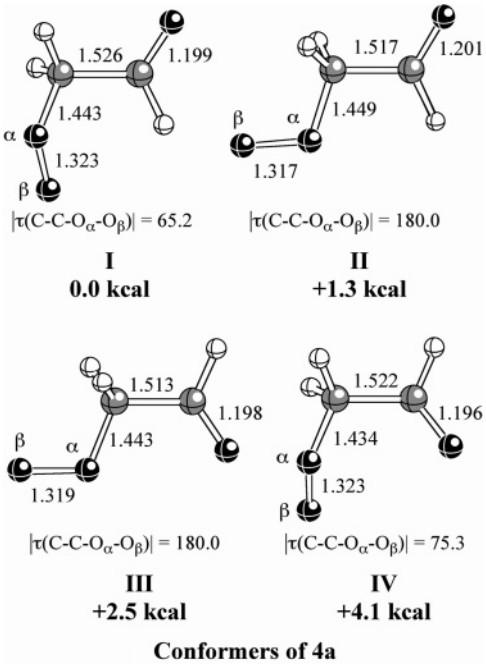

Figure 4. Structures of the 2-oxoethylperoxy radical. Bond lengths (in Å) and torsional angles (in degrees) computed at the B3LYP/6-311G(2d,d,p) level, and relative energies (in kcal/mol) computed with the CBS-QB3 method.

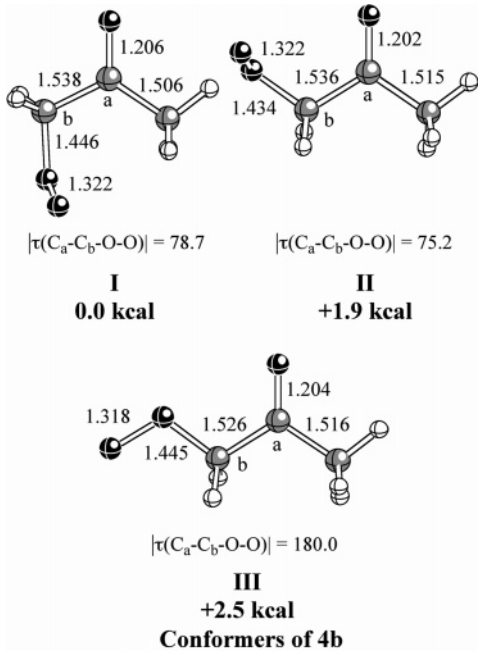

Figure 5. Structures of the 2-oxo-1-propylperoxy (or acetonylperoxy) radical. Bond lengths (in Å) and torsional angles (in degrees) computed at the B3LYP/6-311G(2d,d,p) level, and relative energies (in kcal/mol) computed with the CBS-QB3 method.

Figures 4−6 show the predicted geometries of the oxoalkylperoxy radicals **4a**, **4b**, and **4c**. The 2-oxoethylperoxy radical **4a** has four possible conformers (Figure 4). Structures **I** and **IV**, whose $O_\alpha-O_\beta$ bonds are synclinal to the C−C bonds, possess C−C bonds ~0.01 Å longer than those of structures **II** and **III**, whose $O_\alpha-O_\beta$ and C−C bonds are antiperiplanar. This suggests that in **I** and **IV**, one of the lone pairs on the α-oxygen, which is antiperiplanar to the C−C bond, delocalizes into the σ^*(C−C) orbital (see Scheme 1). This anomeric-like effect, combined with the electrostatic preference for antiparallel C−O

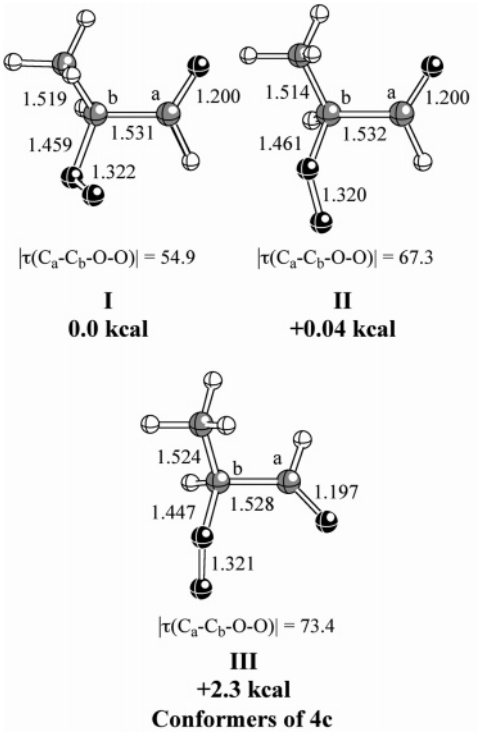

Figure 6. Structures of the 1-oxo-2-propylperoxy radical. Bond lengths (in Å) and torsional angles (in degrees) computed at the B3LYP/6-311G(2d,d,p) level, and relative energies (in kcal/mol) computed with the CBS-QB3 method.

SCHEME 1

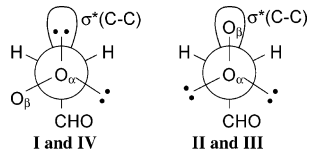

bond dipoles, make **I** the most stable structure. The most stable conformer of the 2-oxo-1-propylperoxy (or acetonylperoxy) radical **4b** (**I**, Figure 5) also benefits both from synclinal O−O and C_a-C_b bonds and from antiparallel C−O bonds. All three conformers of the 1-oxo-2-propylperoxy radical **4c** (Figure 6) have synclinal O−O and C_a-C_b bonds, with the two lowest-energy structures (**I** and **II**) also containing antiperiplanar C−O bond dipoles.

B. Energetics of Vinoxy Oxidation. Table 1 summarizes both our CBS-QB3 and Miyoshi and co-workers'[27] predictions for the energy diagram in Scheme 2. All relative energies are based on the most stable conformer of each species.

Miyoshi and co-workers used RRKM/master equation calculations, based on B3LYP/6-31G(d) molecular parameters, to fit the pressure dependence of the experimental[25−27] second-order rate coefficients for the oxidation reaction. Their simulations also employed G2 calculations of the (experimentally unmeasured) reaction energies. This analysis allowed them to estimate the threshold energy required to dissociate the adduct to vinoxy radical and molecular oxygen.

The G2 reaction energies were added to the threshold energies to derive the forward barriers ($E_{o,rec}$) for the recombination of vinoxy radical and O_2. The negative barriers for **1b** and **1c** are rather surprising, given that transition structures (that is, first-order saddle points) for O_2 addition are predicted by Miyoshi and co-workers to exist on the B3LYP surface at energies above those of the separated reactants. More fundamentally, the loss

TABLE 1: Predictions of Zero-Point-Corrected Energies (kcal/mol) for Scheme 2

system	R_1	R_2	RRKM threshold E[a]	G2 reaction E[a]	$E_{o,rec}$[a]	CBS-QB3 barrier	CBS-QB3 reaction E	adjusted $E_{o,rec}$ [d]
a	H	H	27.6	−26.8	+0.8	+4.3[b]	−22.9[b]	+4.7[c]
b	CH_3	H	28.3	−28.9	−0.6	+2.4[c]	−25.0[c]	+3.3[c]
c	H	CH_3	26.1	−26.9	−0.8	+4.1[c]	−22.6[c]	+3.5[c]

[a] From ref 27. [b] From ref 31. [c] From this work. [d] The sum of the RRKM threshold energy and the CBS-QB3 reaction energy; see the text.

SCHEME 2

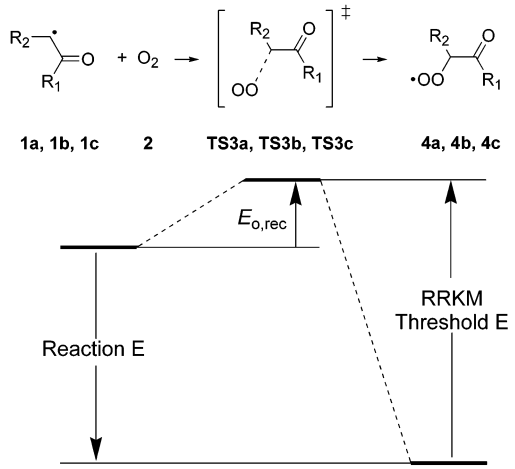

TABLE 2: Theoretical and Experimental Enthalpy Changes (kcal/mol) for Reactions 9, 10, and 11

	ΔH_{298}		
method	reaction 9	reaction 10	reaction 11
B3LYP/6-31G(d,p)	−31.0[a]	−31.6[a]	−32.0[a]
MPW1K/6-31+G(d,p)	−29.6	−31.0	−31.8
CBS-APNO	−32.1	−34.7	−36.7
CBS-QB3	−33.0	−35.6	−37.6
G2	−35.3	−38.6	−41.1
MCG2	−32.3	−35.0	−37.1
G3	−32.2	−35.5	−38.1
CCSD(T)/TZ2P		−31.5[b]	
Blanksby and Ellison[c]	−30.1 ± 1.2	−35.7 ± 2.3	
Knyazev and Slagle[d]	−32.7 ± 0.9	−35.5 ± 2.0	−37.1 ± 2.3

[a] From ref 76; we predict a slightly different value for reaction 9. [b] From ref 77. [c] From refs 73 and 74. [d] From ref 75.

of vinoxy resonance stabilization (see below) required to form the peroxy radicals should lead to an enthalpic barrier.

The prediction of negative barriers for the formation of **4b** and **4c** may be the artifact of a systematic error in the G2 calculations. An overestimate of the exothermicity of the peroxy formation reaction could lower the predicted energy of the transition structure below those of reactants. While there are no experimental thermochemical data on oxoalkylperoxy radicals, such data do exist for a variety of alkylperoxy radicals without oxo groups.[73−75] Table 2 summarizes these data, as well as quantum chemical predictions of ΔH_{298} by us and two other groups,[76,77] for reactions 9−11.

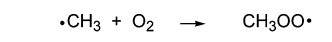

[9]

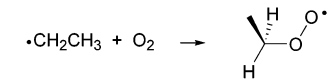

[10]

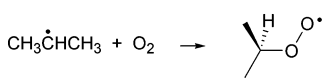

[11]

As compared to Blanksby and Ellison's value[73,74] for ethylperoxy and Knyazev and Slagle's values[75] for all three systems, the B3LYP and MPW1K hybrid density functional methods underestimate the stability of alkylperoxy radicals relative to their O_2 and alkyl radical constituents.[78] The single-level ab initio CCSD(T)/TZ2P calculation of Schaefer and co-workers[77] also underestimates the stability of ethylperoxy radical, as judged by either experimental value. This is despite geometries optimized at the very high CCSD(T)/DZP level.

In contrast, the composite CBS-APNO and CBS-QB3 methods (both used extensively in our previous study[31] of the parent vinoxy radical) predict exothermicities for reactions 9−11 that agree with experiment to within the experimental uncertainties (except for Blanksby and Ellison's[73,74] ΔH_{298} for eq 9). In contrast, the G2 method overestimates the stability of all three alkylperoxy radicals considered. However, if the very same components (except the higher level correction) that are summed to determine the G2 energy are instead summed using Truhlar's MCG2[57,58] weighing coefficients, the resulting reaction energies all agree with experiment. Pople's Gaussian-3 (G3) method[56] also fixes this systematic error in G2.

It is reasonable to assume that G2 also overestimates the stability of oxo-substituted alkylperoxy radicals **4a**, **4b**, and **4c**. This motivates a re-evaluation of the forward barrier for the oxidation of vinoxy radicals **1a**, **1b**, and **1c**. If we combine Miyoshi and co-workers' RRKM threshold energies[27] and our CBS-QB3 reaction energies, we obtain "adjusted" $E_{o,rec}$ values (last column of Table 1) that agree to within 1 kcal/mol of the CBS-QB3 barriers.

Alternatively, it is important to note that Miyoshi and co-workers' prediction of negative barriers for the formation of **4b** and **4c** was based on a scheme which did not include the isomerization of **4b** and **4c** (discussed in sections C and D below). It is possible that a model of the pressure dependence of the experimental[25−27] second-order rate coefficients for the oxidation reaction that included peroxy radical isomerization would lead to positive reaction barriers even with the G2 method.

We also observe that the formation of oxoalkylperoxy radicals is several kcal/mol less exothermic than the formation of the alkylperoxy radicals considered in Table 2. The most important reason for this difference is that adding O_2 to vinoxy radicals causes them to lose resonance stabilization, while adding O_2 to localized alkyl radicals engenders no such loss. To quantify this effect, we propose the following definition of resonance stabilization energy: the difference between (1) the energy required to break the appropriate C−H bond in an aldehyde or ketone to form the delocalized vinoxy radical **1a**, **1b**, or **1c** and (2) the energy required to break the analogous C−H bond in the analogous alcohol. Scheme 3 shows the specific reactions studied, and Table 3 contains the CBS-QB3 energetics.

Table 3 indicates that conjugation in the parent and methyl-substituted vinoxy radicals affords a 7−10 kcal/mol advantage over analogous localized α-hydroxyalkyl radicals. Bouchoux et al.[79] and Espinosa-García et al.[80] have also reported resonance stabilization energies for **1a** and **1b**. However, both groups employ Baird et al.'s[81] original definition in that they compare vinoxy radicals to unsubstituted alkyl radicals. With this approach, they obtain stabilization energies of only 4−6 kcal/mol.

SCHEME 3

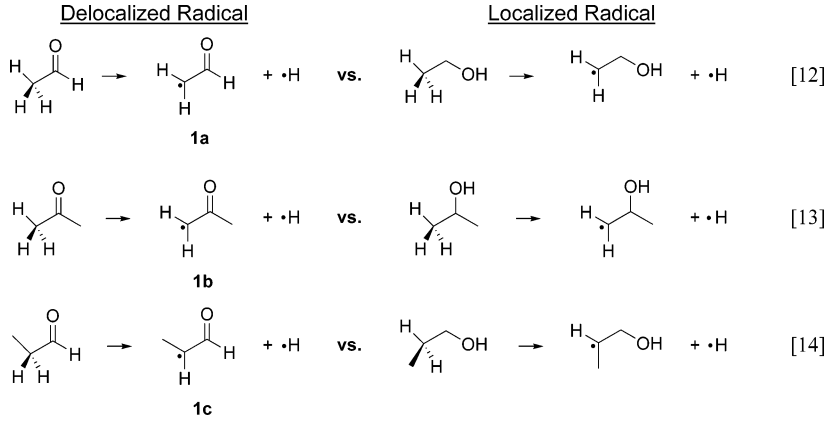

[12] [13] [14]

TABLE 3: CBS-QB3 0 K Reaction Energies (kcal/mol) for Scheme 3

reaction	delocalized ΔE_{rxn}	localized ΔE_{rxn}	resonance ΔE
12	94.0	101.5	−7.5
13	94.9	101.8	−6.9
14	88.8	98.6	−9.8

TABLE 4: CBS-QB3 0 K Relative Energies (kcal/mol) for Hydrogen Shift Reactions 15−21

system	4	TS5	TS6	TS7	8	9	10
a	0.0	+19.5	+39.1		+1.0	−0.7	
b	0.0		+38.4	+26.1		−3.5	+7.4
c	0.0	+18.6	+37.0	+34.9	+1.5	−6.8	+15.1

The oxo group that stabilizes vinoxy radicals **1a**, **1b**, and **1c** has the opposite effect on the peroxy radicals **4a**, **4b**, and **4c**. Brinck et al.[76] predict that such electron-withdrawing groups slightly destabilize peroxy radicals. This effect also helps explain the smaller exothermicity of oxoalkylperoxy radical formation.

C. Intramolecular Hydrogen Shifts in α-Oxoalkylperoxy Radicals. We considered all possible intramolecular hydrogen abstraction reactions for the three oxoalkylperoxy radicals. The parent system **a** can undergo a 1,4-H shift (via **TS5a**) or a 1,3-H shift (via **TS6a**):

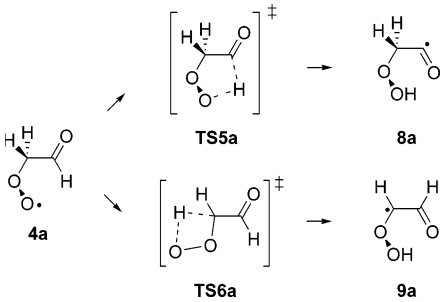

[15] [16]

System **b** can undergo a 1,3-H shift (via **TS6b**) or a 1,5-H shift (via **TS7b**):

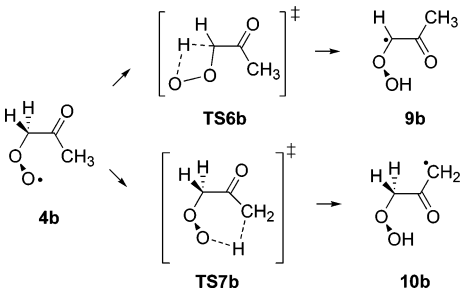

[17] [18]

System **c** can undergo a 1,4-H shift (via **TS5c**), a 1,3-H shift (via **TS6c**), or a 1,5-H shift (via **TS7c**):

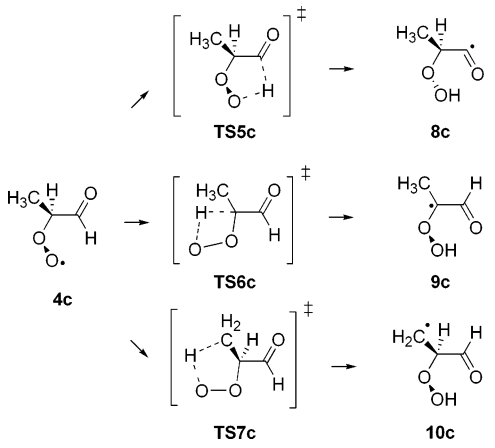

[19] [20] [21]

Figures 7−9 show the geometries of the transition structures for reactions 15−21, and Table 4 contains the energies (relative to reactants **4a**, **4b**, or **4c**) of the most stable conformers of the transition structures and products for these reactions.

The most facile isomerization is the 1,4-shift (**TS5a** and **TS5c**) of the acyl hydrogen, with barriers of 19−20 kcal/mol. The more strained 1,3-hydrogen shift transition structures (**TS6a**, **TS6b**, and **TS6c**) are 18−20 kcal/mol higher in energy. The 1,5-hydrogen shift transition structures (**TS7b** and **TS7c**) are 7−16 kcal/mol higher in energy than **TS5a** and **TS5c**, even though **TS7b** and **TS7c** have less torsional strain. This reflects the fact that acyl C−H bonds are ∼10 kcal/mol weaker than primary C−H bonds.[82] Other correlations between reaction barrier and reaction energy can be seen in the set of 1,3-hydrogen shifts (compare energies of **TS6** and **9**) and the pair of 1,5-hydrogen shifts (compare energies of **TS7** and **10**).

D. Kinetics of Oxoalkylperoxy Radical Isomerization. We solved the master equation for the chemically activated peroxy radicals **4a**, **4b**, and **4c**. Our goal was to quantify the competition between the prompt intramolecular hydrogen shift and the collisional stabilization of **4a**, **4b**, and **4c** as a function of bath gas pressure. Scheme 4 shows the energy diagram treated in the master equation calculations, and Table 5 summarizes the CBS-QB3 threshold energies used.

The entrance channel is the addition of O_2 to a given vinoxy radical, with the initial energy of each oxoalkylperoxy radical being represented by a shifted thermal distribution[30] truncated at threshold energy $E_{o,rev}$. The exit channel is the lowest-barrier

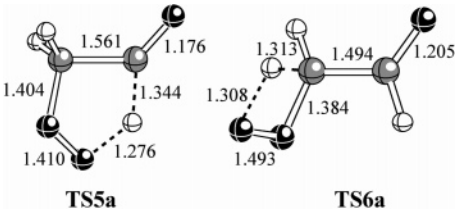

Figure 7. Transition structures for intramolecular hydrogen shifts in the 2-oxoethylperoxy radical. Bond lengths (in Å) computed at the B3LYP/6-311G(2d,d,p) level.

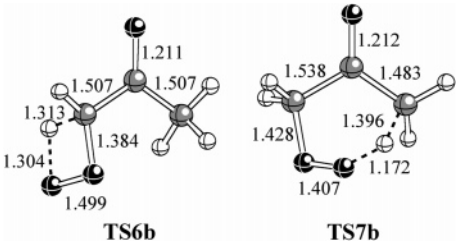

Figure 8. Transition structures for intramolecular hydrogen shifts in the acetonylperoxy radical. Bond lengths (in Å) computed at the B3LYP/6-311G(2d,d,p) level.

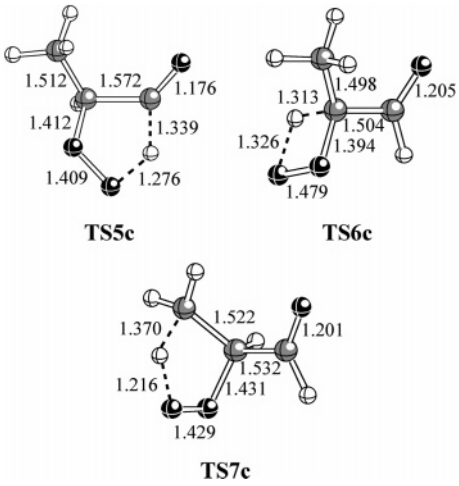

Figure 9. Transition structures for intramolecular hydrogen shifts in the 1-oxo-2-propylperoxy radical. Bond lengths (in Å) computed at the B3LYP/6-311G(2d,d,p) level.

SCHEME 4

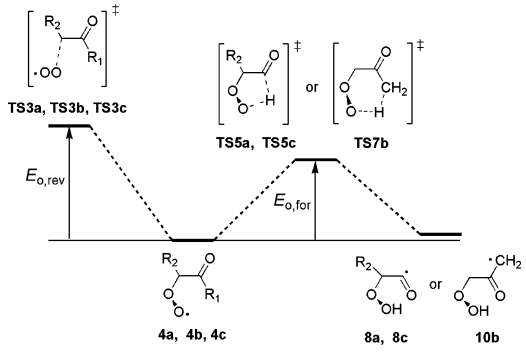

isomerization available to that radical (reactions 15, 18, and 19 above). Reactions 15 and 19 form the hydroperoxyacyl radicals **8a** and **8c**, respectively. Reaction 18 forms the hydroperoxyvinoxy radical **10b**. We assumed in each case that the hydrogen shift was irreversible. (This assumption will be discussed in section E.)

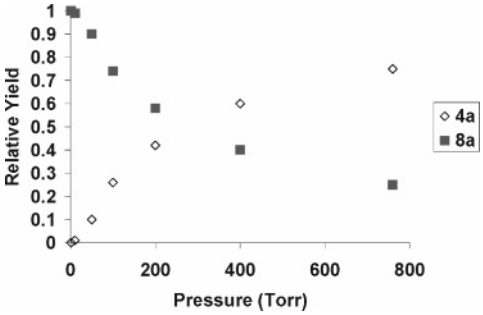

Figure 10. Relative yields of thermalized 2-oxoethylperoxy radical **4a** (◇) and hydroperoxyacetyl radical **8a** (■) predicted by master equation simulations.

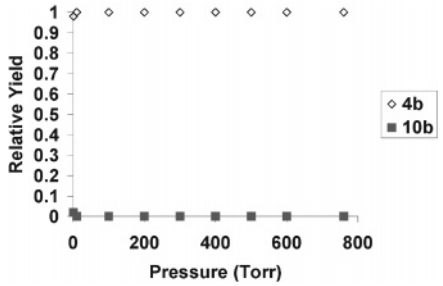

Figure 11. Relative yields of thermalized acetonylperoxy radical **4b** (◇) and 3-hydroperoxyacetonyl radical **10b** (■) predicted by master equation simulations.

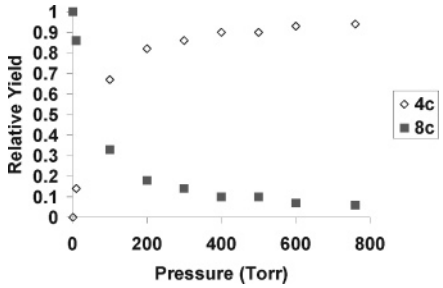

Figure 12. Relative yields of thermalized 1-oxo-2-propylperoxy radical **4c** (◇) and 2-hydroperoxypropanoyl radical **8c** (■) predicted by master equation simulations.

TABLE 5: CBS-QB3 Zero-Point-Corrected Threshold Energies (kcal/mol) for Scheme 4

system	$E_{o,rev}$	$E_{o,for}$
a	+27.3	+19.5
b	+27.4	+26.1
c	+26.7	+18.6

Figures 10−12 show the pseudo steady-state relative yields of thermalized peroxy radical and hydrogen shift product for the three systems. One thousand simulations were run for each bath gas pressure, producing relative yields reproducible to two decimal places.

As we reported earlier,[31] prompt formation of the hydroperoxyacetyl radical **8a** falls off rather slowly with increasing pressure, with ∼25% of **4a** predicted to isomerize even at 1 atm (Figure 10). Prompt formation of the 2-hydroperoxypropanoyl radical **8c** falls off much more rapidly with increasing pressure, with ≤10% of **4c** predicted to isomerize for pressures above 400 Torr (Figure 12). Although **4a** and **4c** have very similar reaction barriers (Table 5), **4c**'s additional methyl group slows its isomerization rate by a factor of ∼3.[83] The 7−8 kcal/mol higher barrier for the methyl hydrogen abstraction in **4b**

TABLE 6: Hydrogen Shift Thermal (298 K) Unimolecular Rate Constants

reactant	A_∞ (s^{-1})	k (s^{-1})
4a	1.61×10^{12}	8.16×10^{-3}
4b	4.39×10^{11}	3.23×10^{-8}
4c	1.60×10^{12}	3.71×10^{-2}

makes the prompt formation of **10b** negligible under all pressures studied (Figure 11). Orlando et al.[84] come to the same conclusion regarding **4b** based on B3LYP/6-31G(d,p) and RRKM calculations.

We tested the sensitivity of our relative yield predictions to a factor of 3 variation in the average energy transferred per collision ($\langle E_d \rangle$) and a ±10% variation in the CBS-QB3 threshold energies (Table 5). These changes caused the 1-atm yield of **8a** to vary from 5% to 70% and the 1-atm yield of **8c** to vary from 0% to 50%. Yields of **10b** remained zero within the uncertainty of our simulations. Variation of the Lennard-Jones parameters by ±20% caused no statistically significant variation in any yields.

We used our CBS-QB3 reaction barriers and B3LYP/6-311G-(2d,d,p)-derived partition functions to estimate the thermal rate constants for the lowest barrier hydrogen shifts. Table 6 shows that all three oxoalkylperoxy radicals will isomerize slowly at 298 K; the shortest lifetime with respect to the hydrogen shift is ~30 s for **4c**. In the atmosphere, all three peroxy radicals, once thermalized, will preferentially undergo bimolecular reactions.

Possible bimolecular reactions of **4a** were discussed previously.[31] The chemistry of **4b** has been rather well-studied.[85] Both the self-reaction of **4b** and its reaction with NO form the chemically activated acetonoxy radical **11**:

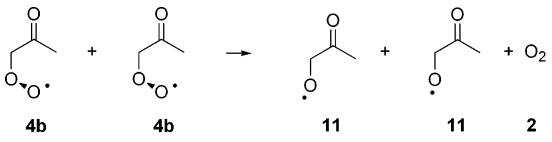

[22]

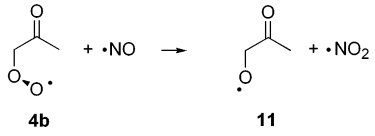

[23]

Calculations by Orlando et al.[84] predict that about 80% of **11** decomposes to acetyl radical and formaldehyde under tropospheric conditions. The chemistry of **4c** has received little attention to date, but workers have proposed reactions similar to eqs 22 and 23.[6,86]

E. Structure and Reactivity of the Hydroperoxyacyl Radical. Figure 13 shows the possible conformers of the acyl radicals **8a** and **8c** formed by prompt isomerization of **4a** and **4c**, as discussed in the previous section. In conformer **I** of both **8a** and **8c**, the intramolecular hydrogen bond overcomes the electrostatic repulsion between synperiplanar C−O bond dipoles. Hydrogen bonding in **8a** confers a net stabilization of 1.7 kcal/mol. In contrast, hydrogen bonding in **8c** confers virtually no net stabilization. One possible reason is that conformer **8c-II**, unlike conformer **8a-II**, benefits from a small dipole−induced dipole interaction between the C═O bond and the synclinal methyl group. (This analysis, due to Wiberg and Martin,[72] was discussed above for the 2-methylvinoxy radical.)

Table 7 summarizes the CBS-QB3 energetics for the lowest barrier decomposition pathways for acyl radicals **8a** and **8c**

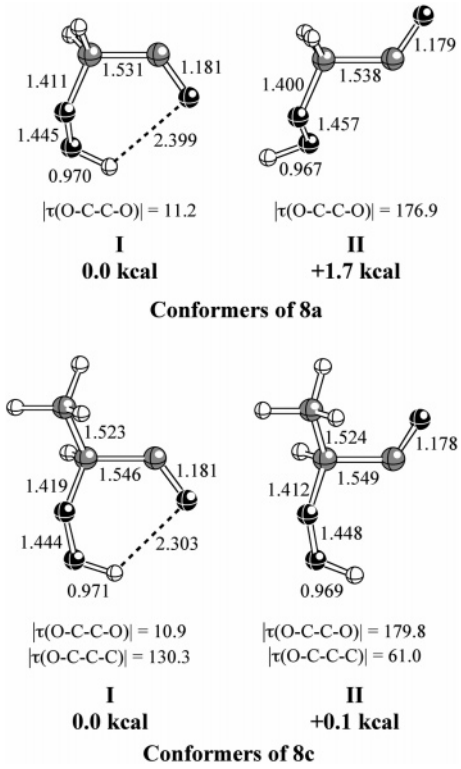

Figure 13. Structures of the hydroperoxyacyl radicals **8a** and **8c**. Bond lengths (in Å) and torsional angles (in degrees) computed at the B3LYP/6-311G(2d,d,p) level, and relative energies (in kcal/mol) computed with the CBS-QB3 method.

TABLE 7: CBS-QB3 0 K Relative Energies (kcal/mol) for Reaction 24

system	8	TS12	13+14	TS15+14	16+17+14
a	0.0	+11.4	+6.4	+5.7	−27.3
c	0.0	+9.7	+6.4	+6.0	−30.6

(reaction 24). Figure 14 shows predicted structures for the C−C

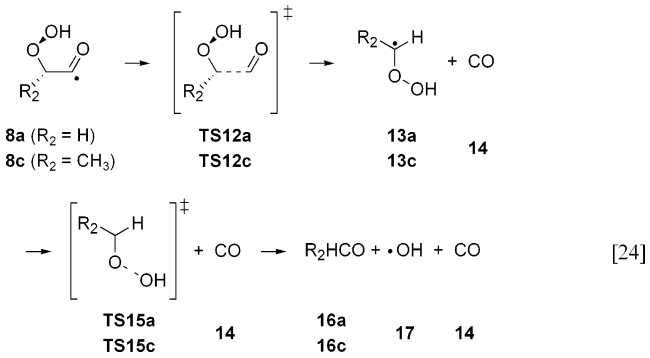

[24]

β-scission transition states (**TS12**), the hydroperoxyalkyl radicals (**13**), and the O−O β-scission transition states (**TS15**).

The methyl substituent in system **c** lowers the energy of **TS12** by ~2 kcal/mol and makes the overall decomposition of the acyl radical more exothermic by ~3 kcal/mol. The methyl substituent also lengthens the C_a-O_b bond by ~0.01 Å throughout the reaction coordinate. As we[31] and others[1,87,88] have noted before, the ipso hydroperoxyalkyl radical (**13**) has an electronic energy only a fraction of a kcal/mol lower than its β-scission transition structure (**TS15**), and the zero-point correction, based on harmonic vibrational frequencies, drops the energy of **TS15** below that of **13**.

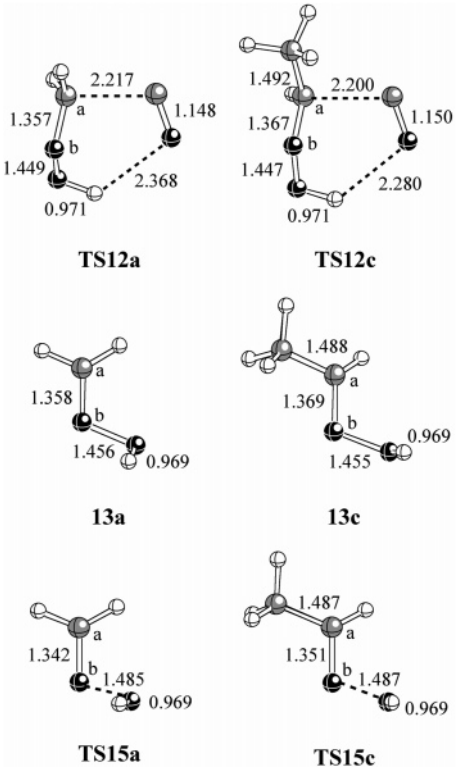

Figure 14. Structures of selected species in reaction 24. Bond lengths (in Å) computed at the B3LYP/6-311G(2d,d,p) level.

The acyl radicals **8a** and **8c** are significantly chemically activated, with internal energy of ≥20 kcal/mol.[31] Moreover, their decomposition transition states **TS12** and **TS15** are rather low in energy and rather high in entropy. It is therefore reasonable to assume that 100% of **8a** and **8c** will decompose promptly under atmospheric conditions to give an equivalent of •OH. Hence, the formation of **8a** and **8c** is irreversible.

F. Formation of •OD Radicals. Finally, we consider our proposal that the 1-oxo-2-propylperoxy radical deuterated at the acyl position (**4c-*d*$_1$**) could be a source of •OD in Kroll et al.'s[34] experiments via reaction 8:

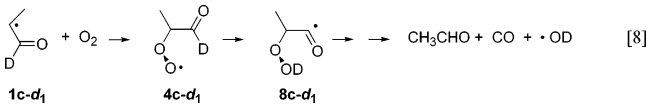

[8]

We performed RRKM/master equation simulations on **4c-*d*$_1$** using the energetics for **4c** (Table 5) and the B3LYP/6-311G-(2d,d,p) moments of inertia and vibrational frequencies for the participating deuterated species (Scheme 5). At 6 Torr (the pressure in Kroll et al.'s LIF experiments), the yield of **8c-*d*$_1$** is ∼100%. As discussed in section E, we can expect all of the **8c-*d*$_1$** to decompose to afford •OD. Therefore, the ozonolysis of 3-hexenes with vinylic deuteriums should produce •OH and •OD radicals in a 1 to 1 ratio. (This assumes that each equivalent of syn propanal oxide produces 1 equivalent of •OH and 1 equivalent of **4c-*d*$_1$** and each equivalent of **4c-*d*$_1$** produces 1 equivalent of •OD.) In contrast, Kroll et al.[34] report •OH/•OD ratios of 2:1 for *cis*-3-hexene and 7:1 for *trans*-3-hexene.

Clearly, our theoretical model significantly overestimates the yield of **8c-*d*$_1$** (and therefore of •OD). A number of factors may contribute to this error: (1) We treat only the lowest-energy conformers in Scheme 5. This simplification underestimates the entropy of intermediate **4c-*d*$_1$** more than the entropy of transition state **TS5c-*d*$_1$** because the oxo group of **4c-*d*$_1$**, unlike that in

SCHEME 5

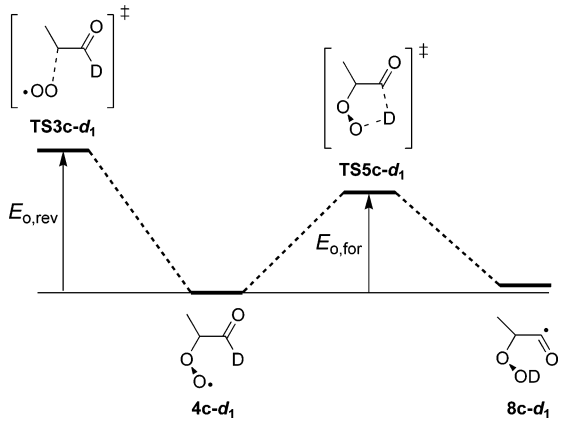

TS5c-*d*$_1$, can be either synperiplanar or antiperiplanar to the peroxy group (Figure 6). A more complete treatment of reactant and transition state conformers, as advocated by Vereecken and Peeters,[63] would therefore decrease the isomerization rate. (2) CBS-QB3 may underestimate the intramolecular hydrogen shift barrier. This is suggested by Coote's recent report[44] that CBS-QB3 predicts lower intermolecular hydrogen abstraction barriers than the very rigorous W1[89] and G3X-RAD[90] methods.

IV. Conclusions

Our B3LYP/6-311G(2d,d,p) calculations indicate that the lowest energy conformers are stabilized by antiparallel bond dipoles, dipole−induced dipole interactions, and delocalization of electron density out of lone pair or antibonding orbitals. For hydroperoxy species such as **8a** and **8c** (Figure 13), intramolecular hydrogen bonding to the carbonyl oxygen more than compensates for the electrostatic repulsion between parallel bond dipoles.

The loss of resonance stabilization in both the parent and methyl-substituted vinoxy radicals impedes their reactivity with O_2 (reaction 2 above). CBS-QB3 calculations predict reaction barriers of 2−4 kcal/mol and reaction energies of −23 to −25 kcal/mol (Table 1). In contrast, the addition of O_2 to unconjugated alkyl radicals is barrierless,[91,92] and reaction energies are several kcal/mol more exothermic (Table 2). Experimental thermochemical data[73−75] for alkylperoxy radicals help validate CBS-QB3 predictions for the energetics of reaction 2. In general, both complete basis set and Gaussian-*n* quantum chemical methods are more reliable for peroxy radicals than single-level ab initio methods, even if the latter employ very high-level ab initio geometries.

The ultimate validation of the CBS-QB3 predictions requires a detailed modeling of the experimental falloff curves for the vinoxy oxidation reactions. Accurate calculation of the vinoxy + O_2 rate constants would require rigorous methods such as variational transition state theory[93] and is beyond the scope of the current investigation.

Experiment[24,25] and theory[1,31] indicate that under atmospheric conditions, the parent vinoxy radical **1a** will be a significant nonphotochemical source of •OH (Figure 10). The 2-methylvinoxy radical **1c** will be a significant •OH source only at low pressures (Figure 12). Larger substituents at the 2-position or alkyl substituents at the 1-position (as in the 1-methylvinoxy radical **1b**) render •OH production from vinoxy radical negligible (Figure 11). Therefore, in alkene ozonolysis, the formation of two equivalents of •OH per equivalent of alkene is an issue only when syn acetaldehyde oxide or syn propanal oxide, the precursors of **1a** and **1c**, is produced.

The production of hydroxyl radical from the oxidation of **1c** provides a qualitative explanation for the observation of •OD in the ozonolysis of 3-hexenes with vinylic deuteriums.[34] A quantitatively accurate master equation simulation would require more rigorous quantum chemistry methods and treatment of all possible conformers. The former is especially important given the high sensitivity of relative yield predictions to small changes in reaction barriers. Moreover, the large difference in the •OH/•OD ratios for *cis*- and *trans*-3-hexene suggests that other factors, such as the difference in the chemical activation of carbonyl oxides formed from *cis*- vs *trans*-3-hexene and the production of •OD from anti carbonyl oxides, must also be considered. Computational studies of the above issues are ongoing.

Acknowledgment. This work was supported by the donors of the American Chemical Society Petroleum Research Fund (K.T.K., No. 38037-GB6; A.S.H., No. 37996-GB6), the NSF Research Site for Educators in Chemistry at the University of Minnesota, the National Computational Science Alliance facility at the University of Kentucky (CHE040003), the University of Minnesota Supercomputing Institute, and the Violet Olson Beltmann Fund of Macalester College. We thank Professor John R. Barker (University of Michigan), Dr. Barron Koralesky (Macalester College), Professor Akira Miyoshi (University of Tokyo), and Professor Jingsong Zhang (University of California, Riverside) for helpful discussions, and K.T.K. thanks Professor Donald G. Truhlar (University of Minnesota) and his research group for their hospitality during a sabbatical visit.

References and Notes

(1) Lee, J.; Bozzelli, J. W. *J. Phys. Chem. A* **2003**, *107*, 3778.
(2) Bozzelli, J. W.; Dean, A. M. *J. Phys. Chem.* **1993**, *97*, 4427.
(3) Slagle, I. R.; Park, J. Y.; Heaven, M. C.; Gutman, D. *J. Am. Chem. Soc.* **1984**, *106*, 4356.
(4) Butkovskaya, N. I.; Kukui, A.; Le Bras, G. *J. Phys. Chem. A* **2004**, *108*, 1160.
(5) Turpin, E.; Fittschen, C.; Tomas, A.; Devolder, P. *J. Atmos. Chem.* **2003**, *46*, 1.
(6) Picquet-Varrault, B.; Doussin, J. F.; Durand-Jolibois, R.; Carlier, P. *J. Phys. Chem. A* **2002**, *106*, 2895.
(7) Tyndall, G. S.; Orlando, J. J.; Wallington, T. J.; Hurley, M. D.; Goto, M.; Kawasaki, M. *Phys. Chem. Chem. Phys.* **2002**, *4*, 2189.
(8) Niki, H.; Maker, P. D.; Savage, C. M.; Breitenbach, L. P.; Hurley, M. D. *J. Phys. Chem.* **1987**, *91*, 941.
(9) Atkinson, R. *J. Phys. Chem. Ref. Data* **1997**, *26*, 215.
(10) Gutbrod, R.; Schindler, R. N.; Kraka, E.; Cremer, D. *Chem. Phys. Lett.* **1996**, *252*, 221.
(11) Gutbrod, R.; Kraka, E.; Schindler, R. N.; Cremer, D. *J. Am. Chem. Soc.* **1997**, *119*, 7330.
(12) Olzmann, M.; Kraka, E.; Cremer, D.; Gutbrod, R.; Andersson, S. *J. Phys. Chem. A* **1997**, *101*, 9421.
(13) Rathman, W. C. D.; Claxton, T. A.; Rickard, A. R.; Marston, G. *Phys. Chem. Chem. Phys.* **1999**, *1*, 3981.
(14) Rickard, A. R.; Johnson, D.; McGill, C. D.; Marston, G. *J. Phys. Chem. A* **1999**, *103*, 7656.
(15) Paulson, S. E.; Chung, M. Y.; Hasson, A. S. *J. Phys. Chem. A* **1999**, *103*, 8125.
(16) Fenske, J. D.; Kuwata, K. T.; Houk, K. N.; Paulson, S. E. *J. Phys. Chem. A* **2000**, *104*, 7246.
(17) Kroll, J. H.; Clark, J. S.; Donahue, N. M.; Anderson, J. G.; Demerjian, K. L. *J. Phys. Chem. A* **2001**, *105*, 1554.
(18) Kroll, J. H.; Sahay, S. R.; Anderson, J. G.; Demerjian, K. L.; Donahue, N. M. *J. Phys. Chem. A* **2001**, *105*, 4446.
(19) Zhang, D.; Zhang, R. *J. Am. Chem. Soc.* **2002**, *124*, 2692.
(20) Zhang, D.; Lei, W.; Zhang, R. *Chem. Phys. Lett.* **2002**, *358*, 171.
(21) Heard, D. E.; Pilling, M. J. *Chem. Rev.* **2003**, *103*, 5163.
(22) Paulson, S. E.; Orlando, J. J. *Geophys. Res. Lett.* **1996**, *23*, 3727.
(23) Hu, J.; Stedman, D. H. *Environ. Sci. Technol.* **1995**, *29*, 1655.
(24) Gutman, D.; Nelson, H. H. *J. Phys. Chem.* **1983**, *87*, 3902.
(25) Lorenz, K.; Rhäsa, D.; Zellner, R.; Fritz, B. *Ber. Bunsen-Ges. Phys. Chem.* **1985**, *89*, 341.
(26) Zhu, L.; Johnston, G. *J. Phys. Chem.* **1995**, *99*, 15114.
(27) Oguchi, T.; Miyoshi, A.; Koshi, M.; Matsui, H.; Washida, N. *J. Phys. Chem. A* **2001**, *105*, 378.
(28) Gilbert, R. G.; Luther, K.; Troe, J. *Ber. Bunsen-Ges. Phys. Chem.* **1983**, *87*, 169.
(29) Curtiss, L. A.; Raghavachari, K.; Trucks, G. W.; Pople, J. A. *J. Chem. Phys.* **1991**, *94*, 7221.
(30) Robinson, P. J.; Holbrook, K. A. *Unimolecular Reactions*; Wiley-Interscience: London, 1972.
(31) Kuwata, K. T.; Templeton, K. L.; Hasson, A. S. *J. Phys. Chem. A* **2003**, *107*, 11525.
(32) Montgomery, J. A., Jr.; Frisch, M. J.; Ochterski, J. W.; Petersson, G. A. *J. Chem. Phys.* **1999**, *110*, 2822.
(33) Montgomery, J. A., Jr.; Ochterski, J. W.; Petersson, G. A. *J. Chem. Phys.* **1994**, *101*, 5900.
(34) Kroll, J. H.; Donahue, N. M.; Cee, V. J.; Demerjian, K. L.; Anderson, J. G. *J. Am. Chem. Soc.* **2002**, *124*, 8518.
(35) Frisch, M. J.; Trucks, G. W.; Schlegel, H. B.; Scuseria, G. E.; Robb, M. A.; Cheeseman, J. R.; Zakrzewski, V. G.; Montgomery, J., A., Jr.; Stratmann, R. E.; Burant, J. C.; Dapprich, S.; Millam, J. M.; Daniels, A. D.; Kudin, K. N.; Strain, M. C.; Farkas, O.; Tomasi, J.; Barone, V.; Cossi, M.; Cammi, R.; Mennucci, B.; Pomelli, C.; Adamo, C.; Clifford, S.; Ochterski, J.; Petersson, G. A.; Ayala, P. Y.; Cui, Q.; Morokuma, K.; Malick, D. K.; Rabuck, A. D.; Raghavachari, K.; Foresman, J. B.; Cioslowski, J.; Ortiz, J. V.; Baboul, A. G.; Stefanov, B. B.; Liu, G.; Liashenko, A.; Piskorz, P.; Komaromi, I.; Gomperts, R.; Martin, R. L.; Fox, D. J.; Keith, T.; Al-Laham, M. A.; Peng, C. Y.; Nanayakkara, A.; Gonzalez, C.; Challacombe, M.; Gill, P. M. W.; Johnson, B.; Chen, W.; Wong, M. W.; Andres, J. L.; Gonzalez, C.; Head-Gordon, M.; Replogle, E. S.; Pople, J. A. *Gaussian 98*, revision A.9 ed.; Gaussian, Inc.: Pittsburgh, PA, 1998.
(36) Becke, A. D. *J. Chem. Phys.* **1993**, *98*, 5648.
(37) Stephens, P. J.; Devlin, F. J.; Chabalowski, C. F.; Frisch, M. J. *J. Phys. Chem.* **1994**, *98*, 11623.
(38) Hehre, W. J.; Ditchfield, R.; Pople, J. A. *J. Chem. Phys.* **1972**, *56*, 2257.
(39) Hariharan, P. C.; Pople, J. A. *Theor. Chim. Acta* **1973**, *28*, 213.
(40) Gonzalez, C.; Schlegel, H. B. *J. Phys. Chem.* **1990**, *94*, 5523.
(41) Gonzalez, C.; Schlegel, H. B. *J. Chem. Phys.* **1989**, *90*, 2154.
(42) Fenske, J. D.; Hasson, A. S.; Paulson, S. E.; Kuwata, K. T.; Ho, A.; Houk, K. N. *J. Phys. Chem. A* **2000**, *104*, 7821.
(43) Cremer, D.; Kraka, E.; Szalay, P. G. *Chem. Phys. Lett.* **1998**, *292*, 97.
(44) Coote, M. L. *J. Phys. Chem. A* **2004**, *108*, 3865.
(45) Lynch, B. J.; Fast, P. L.; Harris, M.; Truhlar, D. G. *J. Phys. Chem. A* **2000**, *104*, 4811.
(46) Lynch, B. J.; Truhlar, D. G. *J. Phys. Chem. A* **2001**, *105*, 2936.
(47) Zhao, Y.; Pu, J.; Lynch, B. J.; Truhlar, D. G. *Phys. Chem. Chem. Phys.* **2004**, *6*, 673.
(48) Jursic, B. S. *J. Mol. Struct. Theochem.* **1998**, *430*, 17.
(49) Malick, D. K.; Petersson, G. A.; Montgomery, J. A., Jr. *J. Chem. Phys.* **1998**, *108*, 5704.
(50) Bartlett, R. J. *J. Phys. Chem.* **1989**, *93*, 1697.
(51) Ochterski, J. W.; Petersson, G. A.; Montgomery, J. A., Jr. *J. Chem. Phys.* **1996**, *104*, 2598.
(52) Gomez-Balderas, R.; Coote, M. L.; Henry, D. J.; Radom, L. *J. Phys. Chem. A* **2004**, *108*, 2874.
(53) Henry, D. J.; Parkinson, C. J.; Radom, L. *J. Phys. Chem. A* **2002**, *106*, 7927.
(54) Guner, V.; Khuong, K. S.; Leach, A. G.; Lee, P. S.; Bartberger, M. D.; Houk, K. N. *J. Phys. Chem. A* **2003**, *107*, 11445.
(55) Parkinson, C. J.; Mayer, P. M.; Radom, L. *Theor. Chem. Acc.* **1999**, *102*, 92.
(56) Curtiss, L. A.; Raghavachari, K.; Redfern, P. C.; Rassolov, V.; Pople, J. A. *J. Chem. Phys.* **1998**, *109*, 7764.
(57) Fast, P. L.; Sanchez, M. L.; Corchado, J. C.; Truhlar, D. G. *J. Chem. Phys.* **1999**, *110*, 11679.
(58) Tratz, C. M.; Fast, P. L.; Truhlar, D. G. *PhysChemComm* **1999**, *2*, 70.
(59) Scott, A. P.; Radom, L. *J. Phys. Chem.* **1996**, *100*, 16502.
(60) Barker, J. R. *MultiWell*, 1.3.2 ed.; University of Michigan: Ann Arbor, MI, July 2003.
(61) Barker, J. R. *Int. J. Chem. Kinet.* **2001**, *33*, 232.
(62) Ayala, P. Y.; Schlegel, H. B. *J. Chem. Phys.* **1998**, *108*, 2314.
(63) Vereecken, L.; Peeters, J. *J. Chem. Phys.* **2003**, *119*, 5159.
(64) Barker, J. R.; Ortiz, N. F. *Int. J. Chem. Kinet.* **2001**, *33*, 246.
(65) Barker, J. R.; Yoder, L. M.; King, K. D. *J. Phys. Chem. A* **2001**, *105*, 796.
(66) Mourits, F. M.; Rummens, F. H. A. *Can. J. Chem.* **1977**, *55*, 3007.
(67) Hippler, H.; Troe, J.; Wendelken, H. J. *J. Chem. Phys.* **1983**, *78*, 6709.
(68) Snider, N. *J. Chem. Phys.* **1984**, *80*, 1885.
(69) Muller, N.; Falk, A. *Ball & Stick 3.8b3, Molecular Graphics Software for MacOS*; Johannes Kepler University: Linz, Austria, 2000.
(70) Williams, S.; Zingher, E.; Weisshaar, J. C. *J. Phys. Chem. A* **1998**, *102*, 2297.

(71) Williams, S.; Harding, L. B.; Stanton, J. F.; Weisshaar, J. C. *J. Phys. Chem. A* **2000**, *104*, 9906.
(72) Wiberg, K. B.; Martin, E. *J. Am. Chem. Soc.* **1985**, *107*, 5035.
(73) Blanksby, S. J.; Ellison, G. B. *Acc. Chem. Res.* **2003**, *36*, 255.
(74) Blanksby, S. J.; Ramond, T. M.; Davico, G. E.; Nimlos, M. R.; Kato, S.; Bierbaum, V. M.; Lineberger, W. C.; Ellison, G. B.; Okumura, M. *J. Am. Chem. Soc.* **2001**, *123*, 9585.
(75) Knyazev, V. D.; Slagle, I. R. *J. Phys. Chem. A* **1998**, *102*, 1770.
(76) Brinck, T.; Lee, H.-N.; Jonsson, M. *J. Phys. Chem. A* **1999**, *103*, 7094.
(77) Rienstra-Kiracofe, J. C.; Allen, W. D.; Schaefer, H. F., III *J. Phys. Chem. A* **2000**, *104*, 9823.
(78) Moreover, Knyazev and Slagle's data demonstrate a 2.8 kcal/mol increase in the stability of ethylperoxy vs methylperoxy, and another 1.6 kcal/mol increase in the stability of isopropylperoxy vs ethylperoxy. The hybrid DFT methods predict at most half of the observed substituent effect. Truhlar and co-workers (Dybala-Defratyka, A.; Paneth, P.; Pu, J.; Truhlar, D. G. *J. Phys. Chem. A* **2004**, *108*, 2475) have recently observed the same problem in B3LYP and MPW1K's treatment of hydrogen transfers between alkyl radicals.
(79) Bouchoux, G.; Chamot-Rooke, J.; Leblanc, D.; Mourgues, P.; Sablier, M. *ChemPhysChem* **2001**, *4*, 235.
(80) Espinosa-Garcia, J.; Marquez, A.; Dobe, S. *Chem. Phys. Lett.* **2003**, *373*, 350.
(81) Baird, N. C.; Gupta, R. R.; Taylor, K. F. *J. Am. Chem. Soc.* **1979**, *101*, 4531.
(82) Afeefy, H. Y.; Liebman, J. F.; Stein, S. E. Neutral Thermochemical Data. In *NIST Chemistry WebBook, NIST Standard Reference Database Number 69, March 2003*; Linstrom, P. J., Mallard, W. G., Eds.; National Institute of Standards and Technology: Gaithersburg MD, 2003.
(83) Our RRKM calculations predict that for internal energies of ~30 kcal/mol, the isomerization rate constants are $k(\mathbf{4a}) = \sim 1.5 \times 10^{10}\ s^{-1}$ and $k(\mathbf{4c}) = \sim 5 \times 10^{9}\ s^{-1}$.
(84) Orlando, J. J.; Tyndall, G. S.; Vereecken, L.; Peeters, J. *J. Phys. Chem. A* **2000**, *104*, 11578.
(85) Tyndall, G. S.; Cox, R. A.; Granier, C.; Lesclaux, R.; Moortgat, G. K.; Pilling, M. J.; Ravishankara, A. R.; Wallington, T. J. *J. Geophys. Res.* **2001**, *106*, 12157.
(86) Tuazon, E. C.; Aschmann, S. M.; Atkinson, R.; Carter, W. P. L. *J. Phys. Chem. A* **1998**, *102*, 2316.
(87) Sumathi, R.; Green, W. H., Jr. *Phys. Chem. Chem. Phys.* **2003**, *5*, 3402.
(88) Niki, H.; Maker, P. D.; Savage, C. M.; Breitenbach, L. P. *J. Phys. Chem.* **1983**, *87*, 2190.
(89) Martin, J. M. L.; Oliveira, G. d. *J. Chem. Phys.* **1999**, *111*, 1843.
(90) Henry, D. J.; Sullivan, M. B.; Radom, L. *J. Chem. Phys.* **2003**, *118*, 4849.
(91) DeSain, J. D.; Klippenstein, S. J.; Miller, J. A.; Taatjes, C. A. *J. Phys. Chem. A* **2003**, *107*, 4415.
(92) Stark, M. S. *J. Phys. Chem. A* **2000**, *122*, 4162.
(93) Truhlar, D. G.; Garrett, B. C.; Klippenstein, S. J. *J. Phys. Chem.* **1996**, *100*, 12771.